

Thermodynamics of $SU(3)$ Lattice Gauge Theory

G. Boyd, J. Engels, F. Karsch, E. Laermann, C. Legeland,
M. Lütgemeier and B. Petersson

Fakultät für Physik, Universität Bielefeld, D-33615 Bielefeld, Germany

Abstract

The pressure and the energy density of the $SU(3)$ gauge theory are calculated on lattices with temporal extent $N_\tau = 4, 6$ and 8 and spatial extent $N_\sigma = 16$ and 32 . The results are then extrapolated to the continuum limit. In the investigated temperature range up to five times T_c we observe a 15% deviation from the ideal gas limit. We also present new results for the critical temperature on lattices with temporal extent $N_\tau = 8$ and 12 . At the corresponding critical couplings the string tension is calculated on 32^4 lattices to fix the temperature scale. An extrapolation to the continuum limit yields $T_c/\sqrt{\sigma} = 0.629(3)$. We furthermore present results on the electric and magnetic condensates as well as the temperature dependence of the spatial string tension. These observables suggest that the temperature dependent running coupling remains large even at $T \simeq 5T_c$. For the spatial string tension we find $\sqrt{\sigma_s}/T = 0.566(13)g^2(T)$ with $g^2(5T_c) \simeq 1.5$.

1 Introduction

The calculation of the equation of state of QCD is one of the central goals of lattice simulations at finite temperature. It has been pursued ever since the first finite temperature Monte Carlo calculations [1]. Besides knowing details about the QCD phase transition like the order and the critical temperature it is of great importance for any investigation of the QCD plasma phase to get a quantitative handle on the equation of state at high temperatures. The intuitive picture of the high temperature phase as a gas of weakly interacting quarks and gluons is based on leading order perturbation theory. However, the well-known infrared problems of perturbative QCD [2] lead to a poor convergence of the corresponding expansion of the thermodynamic potential even at rather high temperatures [3, 4]. Although the newly developed techniques of resummed perturbation theory have led to much progress in perturbative calculations [5], it seems that non-perturbative effects still dominate the equation of state in the temperature regime attainable in future heavy ion experiments.

Lattice calculations of energy density, pressure and other thermodynamic variables have already led to some insight into the temperature dependence of these quantities in the QCD plasma phase. The energy density in the pure gauge theory, for instance, has been found to rise rapidly at T_c and approach the high temperature ideal gas limit from below. However, except for a very recent calculation for the $SU(2)$ gauge theory [6], all studies of the QCD equation of state (EOS) have been performed on rather small lattices. The crucial limitation comes here from the extent of the lattice in Euclidean time (N_τ). So far all calculations of bulk thermodynamic quantities have been restricted to lattices with only four sites in the Euclidean time direction ($N_\tau = 4$) [7]. The small extent of the lattice in the time direction causes large lattice artifacts in thermodynamic quantities. This comes about because the discretization of the field strength tensor in the standard Wilson formulation of lattice QCD [8] introduces $O(a^2)$ deviations from its continuum counterpart, i.e. $O((aT)^2 \equiv N_\tau^{-2})$ corrections at a fixed finite temperature T . In the case of an ideal bose gas – the perturbative high temperature limit of an $SU(N)$ gauge theory – the deviations of bulk thermodynamic quantities like energy density and pressure from the corresponding continuum expressions are as large as 50% on

lattices with only four sites in the time direction. These effects are even larger for a fermi gas [9].

In order to compare lattice calculations of the EOS with continuum perturbation theory or phenomenological models like the bag EOS, it is mandatory to remove the lattice artifacts. This requires a systematic analysis of thermodynamic quantities on lattices with varying N_τ . At fixed temperature T , one can then extrapolate the numerical results to the continuum limit $a \sim 1/N_\tau \rightarrow 0$. The methods required to achieve this have been developed over last few years. In particular, it is now possible to calculate the energy density and pressure non-perturbatively, without using certain perturbative approximations as in earlier calculations [10]. However, since these quantities are measured on the lattice in units of the lattice spacing, e.g. $\epsilon a^4 \sim N_\tau^{-4}$, the statistics required for constant accuracy increases with N_τ correspondingly, i.e. N_τ cannot be chosen too large.

In this paper we present a systematic study of the thermodynamics of the pure gauge sector of QCD, i.e. we neglect the contribution of fermions and study the thermodynamics of a gluon gas, which is described by an $SU(3)$ gauge theory. We calculate thermodynamic quantities on lattices of size $N_\sigma^3 \times N_\tau$ with $N_\tau = 4, 6$ and 8 . In addition, we perform calculations of the string tension on large symmetric lattices of size $32^3 \times 32$, i.e. at zero temperature, in order to set a physical scale for the temperature in our calculations. The results for different values of N_τ are then used to extrapolate to the continuum limit. In the next section we will outline the basic formalism for our calculations. In section 3 we discuss our results for the critical couplings of the deconfinement transition and the string tension at zero temperature. These are used in section 4 to determine the temperature scale for the thermodynamic observables. In section 5 we present our results for pressure, energy density and other thermodynamic quantities and describe their extrapolation to the continuum limit. A discussion of the results and a comparison with continuum models is given in section 6. Part of these results have already been reported in Ref. [11]. Furthermore in section 6 results for the magnetic and electric condensates as well as for the spatial string tension are presented.

2 Thermodynamics on the Lattice

To start the discussion of the thermodynamics of $SU(N)$ gauge theories on the lattice we recall some basic thermodynamic relations in the continuum. All thermodynamic quantities can be derived from the partition function $Z(T, V)$. Its logarithm defines the free energy density,

$$f = -\frac{T}{V} \ln Z(T, V) \quad . \quad (2.1)$$

The energy density and pressure are derivatives of $\ln Z$ with respect to T and V ,

$$\epsilon = \frac{T^2}{V} \frac{\partial \ln Z(T, V)}{\partial T} \quad , \quad (2.2)$$

$$p = T \frac{\partial \ln Z(T, V)}{\partial V} \quad . \quad (2.3)$$

For large, homogeneous systems, however, the pressure can directly be obtained from the free energy density,

$$p = -f \quad . \quad (2.4)$$

Using this relation one can express the entropy density $s = (\epsilon + p)/T$ and the difference between ϵ and $3p$ in terms of derivatives of the pressure with respect to temperature,

$$\frac{\epsilon + p}{T} = \frac{\partial p}{\partial T} \quad , \quad (2.5)$$

$$\epsilon - 3p = T^5 \frac{\partial}{\partial T} (p/T^4) \quad . \quad (2.6)$$

On the lattice, temperature and volume of the thermodynamic system are determined by the lattice size, $N_\sigma^3 \times N_\tau$, and the lattice cut-off a ,

$$T^{-1} = N_\tau a \quad , \quad V = (N_\sigma a)^3 \quad . \quad (2.7)$$

In an $SU(N)$ gauge theory the lattice cut-off a is a function of the bare gauge coupling $\beta \equiv 2N/g^2$. This function fixes the temperature and the physical volume

at a given coupling and is known to two-loop order in perturbation theory. To obtain it non-perturbatively one calculates a physical observable with non-trivial dimension at various values of β on the lattice, i.e. in units of the cut-off. In pure $SU(3)$ gauge theory the string tension σa^2 or the critical temperature $T_c a$ for the deconfinement transition are suitable observables. This then defines the temperature scales $T/\sqrt{\sigma}$ or T/T_c .

Although in principle all thermodynamic quantities can be derived from the free energy density, in practice a direct computation of the partition function on the lattice is not possible. A way out is to calculate the expectation value of the action, i.e. the derivative of $\ln Z$ with respect to the bare gauge coupling β . Up to a normalization constant, resulting from the lower integration limit β_0 , the free energy density is then obtained by integrating this expectation value

$$\frac{f}{T^4}\Big|_{\beta_0}^{\beta} = -N_{\tau}^4 \int_{\beta_0}^{\beta} d\beta' [S_0 - S_T] , \quad (2.8)$$

with $S_0 = 6P_0$ and $S_T = 3(P_{\tau} + P_{\sigma})$. Here $P_{\sigma,\tau}$ denote the expectation values of space-space and space-time plaquettes,

$$P_{\sigma,\tau} = 1 - \frac{1}{N} \text{Re} \langle \text{Tr}(U_1 U_2 U_3^{\dagger} U_4^{\dagger}) \rangle , \quad (2.9)$$

on asymmetric lattices of size $N_{\sigma}^3 \times N_{\tau}$. Similarly, P_0 is the plaquette expectation value on symmetric lattices of size N_{σ}^4 . It serves to normalize the free energy density to be zero at zero temperature. As the physical excitations in the low temperature phase of an $SU(N)$ gauge theory are glueballs, which are known to be quite heavy ($m_G \gtrsim 1$ GeV), the free energy density is expected to drop exponentially ($f \sim \exp(-m_G/T)$). We thus assume that f is negligible below a temperature quite close to T_c . The lower integration limit β_0 can then be chosen correspondingly.

In order to relate the free energy density to the pressure via Eq. 2.4, one has to insure that the spatial volume is large enough. Earlier studies for the $SU(2)$ gauge theory [10] suggest that lattices with spatial size $TV^{1/3} \equiv (N_{\sigma}/N_{\tau}) \geq 4$ are sufficient for this. The difference between ϵ and $3p$ can be derived from Eqs. 2.4, 2.6 and 2.8 as

$$\frac{\epsilon - 3p}{T^4} = N_{\tau}^4 T \frac{d\beta}{dT} [S_0 - S_T] . \quad (2.10)$$

The energy density (ϵ/T^4) is then obtained by adding the result for $3p/T^4$. On isotropic lattices with fixed temporal extent N_τ the variation of the temperature is directly related to the variation of the lattice spacing (Eq. 2.7). The derivative of the bare coupling with respect to T , occurring in Eq. 2.10, thus is connected to the renormalization group equation for the bare coupling,

$$\tilde{\beta}(g) \equiv T \frac{d\beta}{dT} = -a \frac{d\beta}{da} = -2Na \frac{dg^{-2}}{da} \quad . \quad (2.11)$$

We will discuss this relation in the next section.

3 Critical Temperature and the Temperature Scale

3.1 Critical Temperature and the String Tension

In order to express thermodynamic quantities, calculated on the lattice, in physical units we have to find the relation between the gauge coupling β and the lattice cut-off a . This can, for instance, be achieved through a calculation of the critical couplings for the deconfinement transition β_c on lattices with given temporal extent N_τ or a calculation of the string tension $\sqrt{\sigma}a$ at zero temperature. We will present here some new results for both quantities and discuss the determination of the temperature scale from these new calculations as well as further information from MCRG calculations [12] in the next subsection.

We have calculated the critical couplings for the deconfinement phase transition on lattices of size $16^3 \times 4$ and $32^3 \times N_\tau$ with $N_\tau = 6, 8$ and 12 . While the critical couplings on lattices with $N_\tau = 4$ and 6 have been studied with high accuracy in the past [13, 14, 15] those for the larger lattices are known only with much less accuracy. In particular, they have been extracted from calculations on lattices with rather small spatial extent [13, 14] and are therefore expected to be shifted to larger values on the $N_\sigma = 32$ lattices used here.

The critical couplings are determined from an analysis of the Polyakov loop susceptibility,

$$\chi_L = N_\sigma^3 (\langle |L|^2 \rangle - \langle |L| \rangle^2) \quad , \quad (3.1)$$

| N_τ | N_σ | $\beta_c(N_\tau, N_\sigma)$ | $\beta_c(N_\tau, \infty)$ |
|----------|------------|-----------------------------|---------------------------|
| 4 | 16 | 5.6908 (2) | 5.6925 (2) |
| 6 | 32 | 5.8938 (11) | 5.8941 (5) |
| 8 | 32 | 6.0609 (9) | 6.0625 |
| 12 | 32 | 6.3331 (13) | 6.3384 |

Table 1: Critical couplings for the $SU(3)$ deconfinement transition. In the last column we give the extrapolations to the thermodynamic limit ($N_\sigma \rightarrow \infty$). For $N_\tau = 8$ and 12 a finite volume dependence proportional to $(N_\tau/N_\sigma)^3$ was assumed.

with L denoting the lattice average of the Polyakov loop, i.e. the product of link variables in the time direction

$$L = \frac{1}{N_\sigma^3} \sum_{\vec{n}} \frac{1}{N} \text{Tr} \prod_{i=1}^{N_\tau} U_{(\vec{n},i),\hat{0}} \quad . \quad (3.2)$$

The Polyakov loop has been determined at four values of β in the vicinity of the critical point. At each value of the coupling we have performed between 20.000 and 30.000 sweeps - for details of the simulation see the Appendix. Close to the critical point one observes frequent flips between the confined and deconfined phase. In particular for $N_\tau = 8$ we find clear two-peak structures in the Polyakov-loop distribution functions, which support the first order nature of the transition.

To determine the critical point we have interpolated the results at the four couplings with the density of states method (DSM) [16]. Pronounced peaks in the Polyakov loop susceptibilities are visible for all four lattice sizes. In Figure 1 we show the susceptibilities for the two larger lattices, $32^3 \times 8$ and $32^3 \times 12$, in a narrow region around the peak location. The critical couplings and their errors have been determined from a jackknife analysis for the maxima of the susceptibilities. These errors are shown as horizontal bars in Figure 1, all critical couplings are listed in Table 1.

For the $N_\tau = 4$ and 6 lattices our analysis of the critical couplings is in complete agreement with earlier determinations [15]. For $N_\tau = 8$ and 12 we obtain, however, significantly larger critical couplings than those found in previous calculations [13,

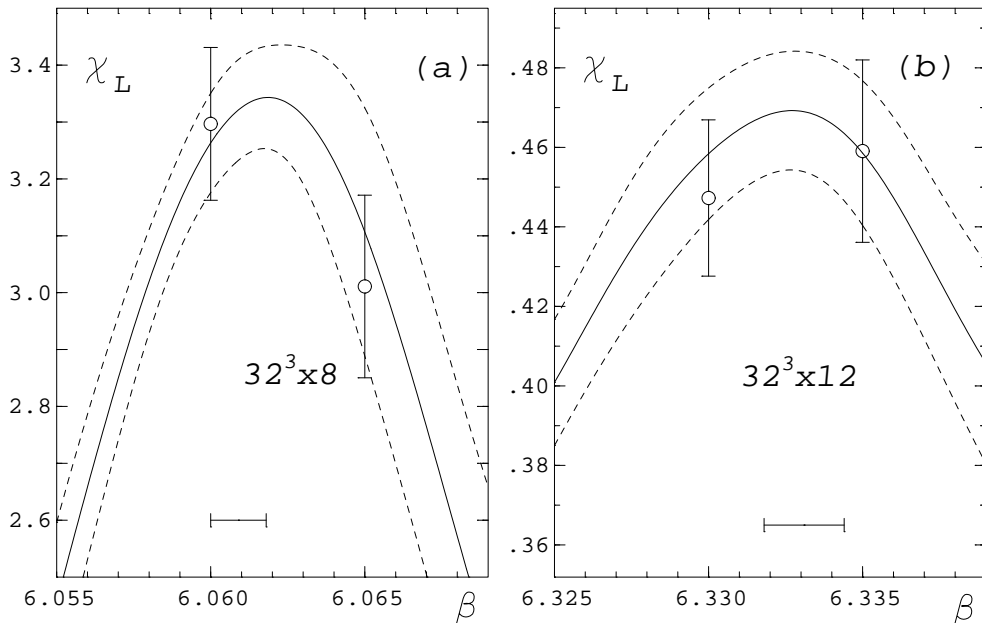


Figure 1: The Polyakov-loop susceptibility on lattices of size $32^3 \times 8$ (a) and $32^3 \times 12$ (b). The solid curves are the DSM interpolations, the dashed lines show the jackknife error bands. The interpolations are based on data collected at $\beta = 6.04, 6.06, 6.065, 6.07$ and 6.08 (a) and $\beta = 6.32, 6.33, 6.335$ and 6.34 (b), respectively.

14]. The shift towards larger values is expected and due to our larger spatial volume. In the analysis of the critical couplings for $N_\tau = 4$ and 6 a clear shift towards larger values of β_c has been observed with increasing spatial volume. In fact, as the transition is first order for the $SU(3)$ gauge theory, the critical couplings will scale like

$$\beta_c(N_\tau, N_\sigma) = \beta_c(N_\tau, \infty) - h \left(\frac{N_\tau}{N_\sigma} \right)^3. \quad (3.3)$$

Using Eq. 3.3 with the constant $h \lesssim 0.1$ determined from the analysis at $N_\tau = 6$ [15] one can extrapolate our critical couplings to the thermodynamic limit. This amounts to a shift of the critical coupling by about about 0.0016 for $N_\tau = 8$ and 0.0053 for $N_\tau = 12$. The resulting values are given in the last column of Table 1.

In order to determine an absolute scale for the temperature we have to evaluate a physical observable which is known experimentally. A suitable quantity for calculations in the pure gauge sector of QCD is the string tension. At the critical couplings

| N_τ | β_c | $\sqrt{\sigma}a$ | $T_c/\sqrt{\sigma}$ |
|----------|-------------|------------------|---------------------|
| 4 | 5.6925 (2) | 0.4179 (24) | 0.5983 (30) |
| 6 | 5.8941 (5) | 0.2734 (37) | 0.6096 (71) |
| 8 | 6.0609 (9) | 0.1958 (17) | 0.6383 (55) (+13) |
| 12 | 6.3331 (13) | 0.1347 (6) | 0.6187 (28) (+42) |

Table 2: The string tension at the critical couplings for the deconfinement transition and the ratio $T_c/\sqrt{\sigma}$.

determined for $N_\tau = 8$ and 12 we have calculated the string tension on lattices of size 32^4 using standard smearing techniques to evaluate the heavy quark potential. For this analysis we have generated 500 gauge field configurations separated by 10 sweeps. In these cases results for the string tension are summarized in Table 2 where we also give the resulting critical temperature in units of the string tension. For $N_\tau = 4$ and 6 the ratio $T_c/\sqrt{\sigma}$ has been evaluated at the critical couplings extrapolated to the infinite volume limit. Results for the string tension have been taken from Ref. [17] and have been interpolated at β_c . For $N_\tau = 8$ and 12 we evaluate this ratio at the critical couplings determined by us on lattices with finite N_σ/N_τ . The volume dependence of $T_c/\sqrt{\sigma}$, resulting from a shift of the critical couplings, is taken into account as a systematic error, which we estimate by assuming an exponential scaling of $\sqrt{\sigma}a$ according to the asymptotic renormalization group equation. It is also given in the last column of Table 2.

Although the ratio hardly shows a systematic cut-off dependence, we have extrapolated the results for the different N_τ -values to the continuum limit using a fit of the form $a_0 + a_2/N_\tau^2$. This yields

$$\frac{T_c}{\sqrt{\sigma}} = 0.625 \pm 0.003 (+0.004) . \quad (3.4)$$

The number in brackets indicates the systematic shift we expect from the infinite volume extrapolation of the critical couplings. Using $\sqrt{\sigma} = 420\text{MeV}$ this gives a critical temperature of about 260 MeV. We note that this estimate of T_c is about 10% larger than earlier estimates [18], which is due to our newly determined critical couplings for the larger lattices.

3.2 The Temperature Scale

The calculation of a physical quantity like $\sqrt{\sigma}a$ fixes the lattice cut-off and thus the temperature at a given value of the gauge coupling. On a lattice with temporal extent N_τ the temperature can then be expressed in units of the string tension and is given by $T/\sqrt{\sigma} = 1/\sqrt{\sigma}aN_\tau$. This is, in principal, sufficient to perform all thermodynamic calculations we are going to discuss in the next sections. In practice, however, it is much more convenient to work with a direct parameterization of the relation between the cut-off and the gauge coupling. This will largely simplify the calculation of quantities that involve derivatives with respect to the temperature (see for instance Eq. 2.10).

In the asymptotic scaling regime the relation between cut-off and gauge coupling is given by the universal terms of the QCD β -function, $a\Lambda_L = R(\beta)$, with

$$R(\beta) = \left(\frac{\beta}{2Nb_0} \right)^{b_1/2b_0^2} \exp[-\beta/4Nb_0] \quad , \quad (3.5)$$

and the coefficients, for a vanishing number of quark flavours,

$$b_0 = \frac{11N}{48\pi^2} \quad , \quad b_1 = \frac{34}{3} \left(\frac{N}{16\pi^2} \right)^2 \quad . \quad (3.6)$$

However, it is well-known that in the coupling regime close to $g^2 = 1$, which one is usually exploring in lattice calculations, there are large deviations from the asymptotic scaling relation. Still it seems that a unique relation between the gauge coupling and the lattice cut-off can be established in this intermediate coupling regime to the extent that scaling violations in ratios of physical observables are small. The major part of the observed deviations from asymptotic scaling can be taken care of through a replacement of the bare coupling by a renormalized coupling [19]. We will use here the definition

$$\beta_{\text{eff}} = \frac{3(N^2 - 1)}{2S_0} \quad . \quad (3.7)$$

With this relation one can determine the cut-off as

$$a\Lambda_L = R(\beta_{\text{eff}})e^{\pi^2(0.089139 - 3/(22N^2))} \quad (3.8)$$

The deviations from the asymptotic relation given in Eq. 3.5 have recently been analyzed for the $SU(3)$ gauge theory in great detail using a MCRG analysis of ratios of Wilson loops [12]. Here one calculates the change in the gauge coupling needed to change the lattice cut-off by a factor two,

$$\Delta\beta \equiv \beta(a) - \beta(2a) \quad (3.9)$$

The resulting $\Delta\beta$ -function is shown in Figure 2 together with $\Delta\beta$ values extracted from calculations of the critical couplings for the deconfinement transition, $\Delta\beta = \beta_c(2N_\tau) - \beta_c(N_\tau)$. As can be seen from this figure, the use of an effective coupling, together with the asymptotic scaling relation, describes the structure of the observed scaling violations qualitatively correctly (dashed curve). Yet, in the region below

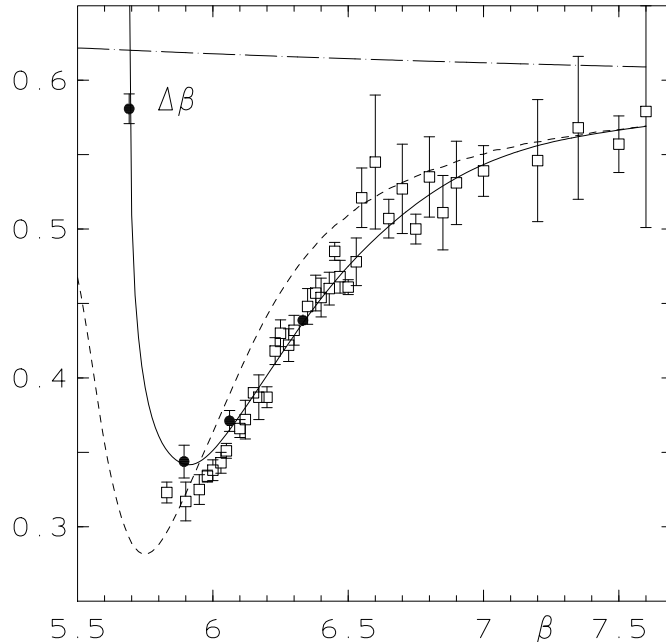


Figure 2: The $\Delta\beta$ -function, Eq. 3.9, from results of MCRG studies [12] (squares) and from our finite temperature calculation (dots). The dashed (dashed-dotted) curve shows $\Delta\beta$ as obtained from the asymptotic form of the renormalization group equation using the effective (bare) coupling. The solid curve is derived from our ansatz, Eq. 3.10.

$\beta \simeq 6.5 - 7$ there are still considerable deviations from the data. In order to get a

quantitative description we use therefore the ansatz

$$a\Lambda_L = R(\beta) \cdot \lambda(\beta) \quad , \quad (3.10)$$

and determine the function $\lambda(\beta)$ from the measurements of the critical couplings for $N_\tau = 4, 6, 8, 12$ (Table 1) and for $N_\tau = 3$ from Ref. [18]. The critical temperature

$$T_c = \frac{1}{N_\tau a(\beta_c)} \quad (3.11)$$

must be independent of the coupling. The function $\lambda(\beta)$ is then obtained at the critical couplings from

$$\lambda(\beta_c) = \frac{1}{N_\tau R(\beta_c) \cdot T_c / \Lambda_L} \quad , \quad (3.12)$$

up to the unknown constant T_c / Λ_L . We have fixed this constant to

$$T_c / \Lambda_L = 34.38 \quad , \quad (3.13)$$

by first interpolating $1/N_\tau R(\beta_c)$ in β and then requiring a smooth transition of the resulting $\Delta\beta$ -function into that of the effective coupling scheme at higher β -values. This is shown as solid curve in Figure 2. Quite obviously, both the critical couplings and $\Delta\beta$ are reproduced above $\beta \approx 6.0$ very well by the introduction of one correction function $\lambda(\beta)$. At smaller β -values, however, we observe differences.

In Table 3 we give our results for the function $\lambda(\beta)$, which allows a direct evaluation of the lattice cut-off $a\Lambda_L$ from Eq. 3.10. Knowing the cut-off as a function of the gauge coupling β we can also evaluate the derivative $ad\beta/da$, which is needed for the calculation of the difference $\epsilon - 3p$ (Eq. 2.10). The corresponding values are also given in Table 3.

4 Thermodynamics on Finite Lattices: $N_\tau=4, 6$ and 8

| $\beta = 2N/g^2$ | λ | adg^{-2}/da | $\partial g_{\sigma}^{-2}/\partial \xi$ | $\partial g_{\tau}^{-2}/\partial \xi$ |
|------------------|-----------|---------------|---|---------------------------------------|
| 5.70 | 2.194700 | -0.077855 | 0.378981 | -0.340054 |
| 5.75 | 2.087578 | -0.079269 | 0.372659 | -0.333024 |
| 5.80 | 1.990720 | -0.081694 | 0.366500 | -0.325653 |
| 5.85 | 1.905342 | -0.085053 | 0.360557 | -0.318030 |
| 5.90 | 1.831481 | -0.089150 | 0.354868 | -0.310293 |
| 5.95 | 1.768642 | -0.093699 | 0.349471 | -0.302621 |
| 6.00 | 1.715383 | -0.098172 | 0.344400 | -0.295314 |
| 6.05 | 1.670045 | -0.102343 | 0.339672 | -0.288501 |
| 6.10 | 1.631051 | -0.105965 | 0.335221 | -0.282238 |
| 6.15 | 1.596995 | -0.109147 | 0.330959 | -0.276386 |
| 6.20 | 1.567082 | -0.112127 | 0.326800 | -0.270737 |
| 6.25 | 1.540692 | -0.114874 | 0.322688 | -0.265252 |
| 6.30 | 1.517309 | -0.117373 | 0.318698 | -0.260011 |
| 6.35 | 1.496477 | -0.119668 | 0.314933 | -0.255099 |
| 6.40 | 1.477892 | -0.121832 | 0.311500 | -0.250584 |
| 6.45 | 1.461275 | -0.123799 | 0.308467 | -0.246568 |
| 6.50 | 1.446329 | -0.125501 | 0.305763 | -0.243012 |
| 6.55 | 1.432777 | -0.127015 | 0.303276 | -0.239769 |
| 6.60 | 1.420468 | -0.128442 | 0.300900 | -0.236679 |
| 6.65 | 1.409274 | -0.129750 | 0.298556 | -0.233681 |
| 6.70 | 1.399057 | -0.130908 | 0.296289 | -0.230835 |
| 6.75 | 1.389672 | -0.131888 | 0.294178 | -0.228235 |
| 6.80 | 1.380963 | -0.132664 | 0.292300 | -0.225968 |
| 6.85 | 1.372792 | -0.133297 | 0.290707 | -0.224058 |
| 6.90 | 1.365080 | -0.133855 | 0.289355 | -0.222428 |
| 6.95 | 1.357773 | -0.134348 | 0.288176 | -0.221001 |
| 7.00 | 1.350826 | -0.134792 | 0.287100 | -0.219704 |
| 7.05 | 1.344204 | -0.135196 | 0.286069 | -0.218471 |
| 7.10 | 1.337881 | -0.135574 | 0.285065 | -0.217278 |
| 7.15 | 1.331835 | -0.135921 | 0.284078 | -0.216117 |
| 7.20 | 1.326041 | -0.136234 | 0.283100 | -0.214983 |
| ∞ | 1.000000 | -0.139316 | 0.201600 | -0.131940 |

Table 3: The correction factor λ and non-perturbative coupling derivatives.

4.1 Perturbative High Temperature Limit

In order to extract physical observables in the continuum limit from results on finite lattices at finite lattice cut-off one has to control the infrared as well as ultraviolet effects that influence them. In the case of thermodynamic observables infrared and ultraviolet effects are of importance in different temperature regimes. Close to the phase transition low momentum modes are most dominant and the finite physical volume thus influences physical observables strongly. In this regime thermodynamic quantities strongly depend on $TV^{1/3} \equiv N_\sigma/N_\tau$. This has been shown for the $SU(2)$ theory [6] and was used there to extract the critical energy density in the thermodynamic limit.

At high temperature, high momentum modes ($|\vec{p}| \sim T$) give the largest contribution to the energy density and pressure, at least to the extent that the momentum spectrum is well approximated by that of an ideal gas. This contribution is therefore strongly influenced by the finite lattice cut-off. The standard one-plaquette Wilson action used in lattice calculations provides a discrete version of the field strength tensor, which leads to deviations of $O(a^2)$ of the lattice Lagrangian from its continuum counterpart. Thermodynamic observables like energy density and pressure will then deviate from the continuum values by $O((aT)^2)$ terms (note that $aT \equiv 1/N_\tau$). For a non-interacting gluon gas, which corresponds to the $g^2 \rightarrow 0$ limit of the finite temperature $SU(N)$ gauge theory, one finds explicitly [6, 20]

$$\frac{\epsilon}{T^4} = \frac{3p}{T^4} = (N^2 - 1) \frac{\pi^2}{15} \left[1 + \frac{30}{63} \cdot \left(\frac{\pi}{N_\tau} \right)^2 + \frac{1}{3} \cdot \left(\frac{\pi}{N_\tau} \right)^4 + O\left(\frac{1}{N_\tau^6} \right) \right]. \quad (4.1)$$

Apparently the subleading corrections are still large for lattices with small temporal extent like $N_\tau = 4$. We therefore will restrict our extrapolations to the continuum limit ($N_\tau \rightarrow \infty$) to the numerical results obtained on lattices with temporal extent $N_\tau = 6$ and 8. We will work on large spatial lattices, $N_\sigma/N_\tau = (4 - 5.33)$, which will ensure that we are close to the thermodynamic limit for a wide temperature range except very close to T_c .

4.2 Monte Carlo Results

As explained in section 2, the basic observable entering the calculations of the pressure is the difference between the expectation values of the action densities calculated at zero temperature ($N_\tau = N_\sigma$) and at finite temperature ($N_\tau < N_\sigma$). For dimensional reasons these differences will scale like N_τ^{-4} . We thus consider the quantities

$$\Delta S = N_\tau^4(S_0 - S_T) . \quad (4.2)$$

Due to the strong N_τ -dependence of ΔS a high accuracy of the plaquette expectation values is needed. We have calculated plaquette expectation values on lattices of size 16^4 , 32^4 as well as $16^3 \times 4$, $32^3 \times 6$ and $32^3 \times 8$ for a large number of gauge couplings. A collection of all our results as well as further information about the actual Monte Carlo calculation is given in the Appendix.

In Figure 3 we show the differences ΔS for $N_\tau = 4, 6$ and 8 . As can be seen their magnitude remains $O(1)$ with increasing N_τ . Note, however, a drop of the maximum of the plaquette difference with increasing N_τ as well as a widening of the peak as function of β . Both effects reflect the presence of finite cut-off effects, which will show up in the pressure as well as the energy density calculated from ΔS .

For a calculation of the pressure we have to integrate ΔS with respect to β . In order to estimate the error resulting from this integration we performed it in two different ways. The most straightforward way is to use a straight line interpolation between neighbouring data points. We may, however, make use of the fact that the values of ΔS calculated at different values of β are statistically independent and use a (spline) interpolating curve to smoothen statistical fluctuations. These smooth interpolations are shown in Fig. 3. We also see in this figure that ΔS rapidly becomes small below the critical coupling $\beta_c(N_\tau, N_\sigma)$. We thus can use a value β_0 close to β_c for the normalization of the free energy density and calculate the pressure by integrating the plaquette differences as given in Eq. 2.8.

In order to represent the pressure in terms of T/T_c we will use the two parametrizations (Eqs. 3.8 and 3.10) discussed in the previous section. This will give us some idea about the systematic errors induced through such a parametrization. In the

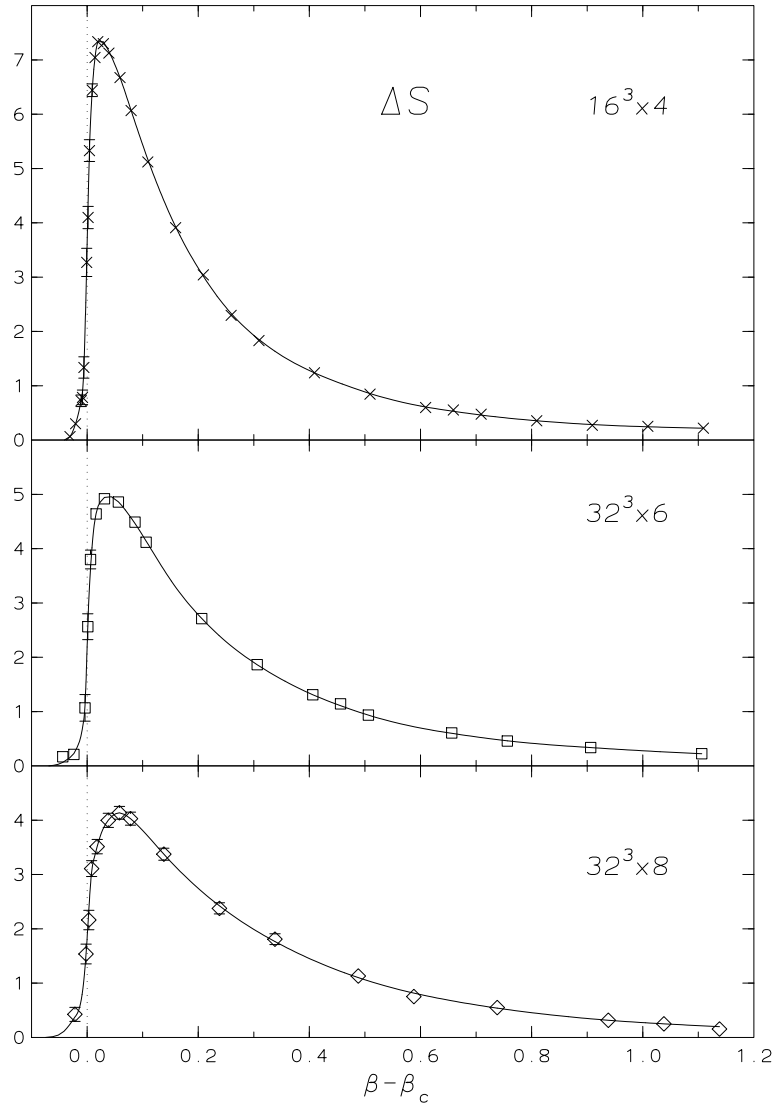


Figure 3: The difference ΔS versus $\beta - \beta_c(N_\tau, N_\sigma)$ for $N_\tau = 4, 6$ and 8 .

case of the pressure a change in the parametrization will only amount to a shift in the temperature scale. This effect is largest for small values of N_τ .

The results for the pressure as a function of T/T_c obtained from calculations with temporal extent $N_\tau = 4, 6$ and 8 are shown in Figure 4. We clearly see the expected finite size dependence. It qualitatively reflects the N_τ -dependence of the free gluon gas, which is shown by horizontal dashed-dotted lines in this figure. Quantitatively, however, we find that the cut-off dependence of the pressure is considerably weaker than suggested by the free gas calculation. We will discuss this in detail in the next section.

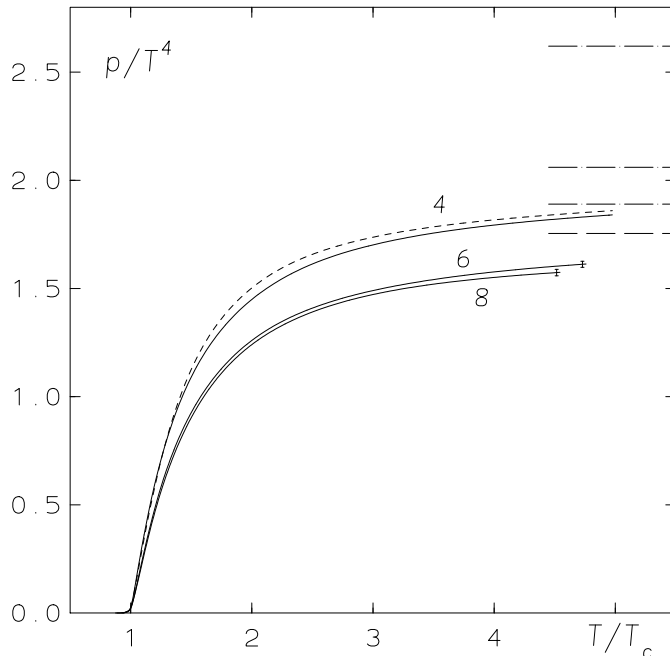


Figure 4: The pressure versus T/T_c for $N_\tau = 4, 6$ and 8 integrating the interpolations for the action density. For $N_\tau = 4$ we show two curves, one for the temperature scale using the effective coupling scheme (dashed curve) and one for our parametrization (solid curve). For $N_\tau = 6$, and 8 we only show the latter. The error bars indicate the uncertainties arising from the integration. The horizontal dashed line shows the ideal gas continuum value, the dashed-dotted lines the corresponding lattice values for $N_\tau = 4, 6$ and 8 .

Unlike the pressure, the absolute magnitude of the energy density depends on the derivative $Td\beta/dT$. Again we will observe the strongest sensitivity to the parametrization of the temperature scale in the $N_\tau = 4$ case, where the numerical calculations close to T_c are performed with bare couplings $\beta \in [5.6, 5.8]$, i.e. in the region of strongest variation of the cut-off with β (dip in the $\Delta\beta$ -function). In Fig. 5 we show the difference $(\epsilon - 3p)/T^4$ obtained with the parametrization of the temperature scale specified in Eq. 3.10. For $N_\tau = 6$ and 8 the influence of the parametrization is not significant and is well inside the error bars of the data.

The first order nature of the $SU(3)$ phase transition has clearly been established in the studies on lattices with $N_\tau = 4$ and 6 and the latent heat at T_c has been estimated in these cases [15]. Also in our calculations for $N_\tau = 8$ and 12 we see clear metastabilities (phase flips of the Polyakov loop) at the critical coupling. Our statis-

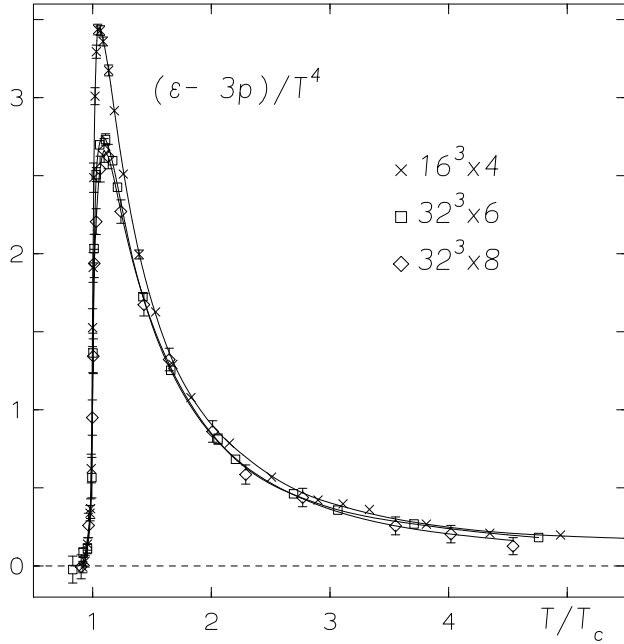


Figure 5: The difference $(\epsilon - 3p)/T^4$.

tics were, however, not sufficient to extract the latent heat from the discontinuity in the plaquette expectation values. We thus did not attempt to separate our data sample in the vicinity of β_c into sets belonging to different phases. Consequently our interpolation curves for $(\epsilon - 3p)/T^4$, shown in Fig. 5, are continuous (as it should be for calculations performed in finite physical volumes).

Combining the results for the pressure and the difference $\epsilon - 3p$ we can calculate the energy density. This is shown in Fig. 6 for the three different lattice sizes.

5 Thermodynamics in the Continuum Limit

Based on the analysis of the pressure and energy density on various size lattices, which we have presented in the previous section, we can attempt now to extrapolate these quantities to the continuum limit. As discussed in the previous section, the leading corrections to the continuum limit are $O(N_\tau^{-2})$. The analysis of the high temperature ($g^2 = 0$) ideal gas limit, however, shows that for $N_\tau = 4$ higher order corrections are expected to be very important. We thus will perform an extrapola-

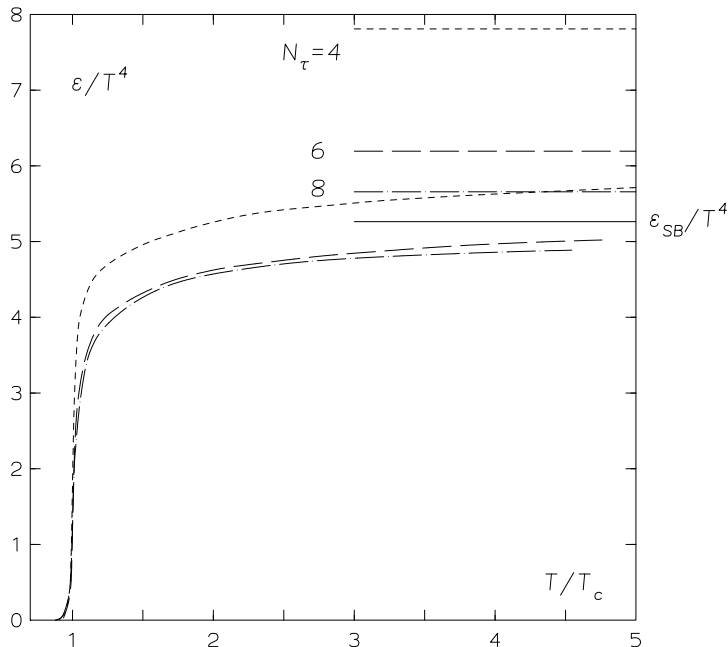


Figure 6: The energy density versus T/T_c for $N_\tau = 4$ (short dashes), 6 (dash-dotted line) and 8 (long dashes).

tion to the continuum limit only on the basis of our numerical results for $N_\tau = 6$ and 8. We have performed extrapolations using the ansatz,

$$\left(\frac{p}{T^4}\right)_a = \left(\frac{p}{T^4}\right)_0 + \frac{c_2(T)}{N_\tau^2} \quad , \quad (5.1)$$

We generally find that the difference between the extrapolated values and the results for $N_\tau = 8$ is less than 3%, which should be compared with the corresponding result for the free gas, where the difference is still about 10%. At our highest temperatures, $T/T_c \simeq 4 - 5$, the fit parameter c_2 takes values which are only half as large as the expansion parameter for an ideal gas (Eq. 4.1).

The cut-off dependence in $(\epsilon - 3p)/T^4$ is much smaller than for the pressure alone. Within errors the interpolation curves shown for $N_\tau = 6$ and 8 in Fig. 5 are already coinciding. Combining therefore $(\epsilon - 3p)/T^4$ for $N_\tau = 8$ and the extrapolations for the pressure we obtain the continuum results for other thermodynamic quantities like the energy density and entropy density, $s = (\epsilon + p)/T$. These results are summarized in Fig. 7.

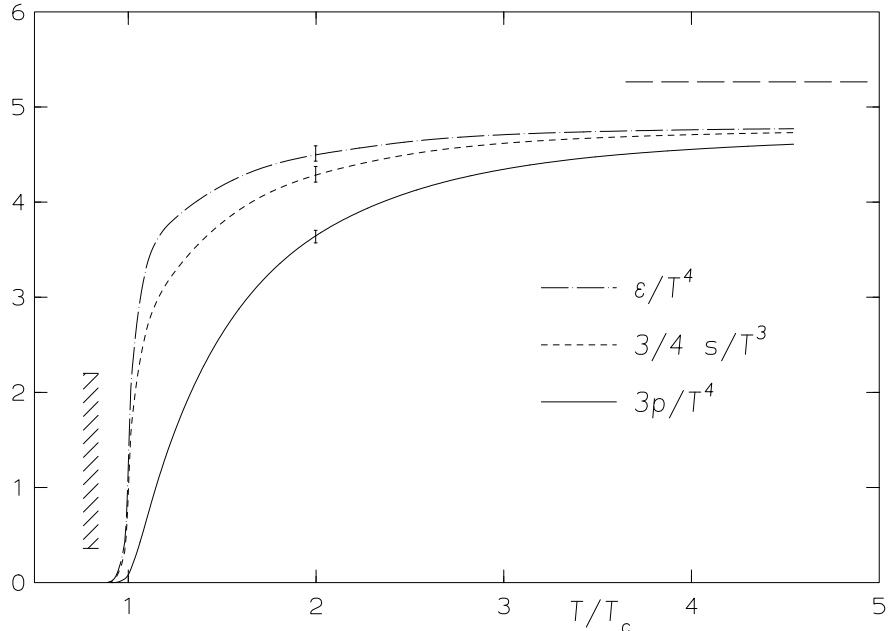


Figure 7: Extrapolation to the continuum limit for the energy density, entropy density and pressure versus T/T_c . The dashed horizontal line shows the ideal gas limit. The hatched vertical band indicates the size of the discontinuity in ϵ/T^4 (latent heat) at T_c [15]. Typical error bars are shown for all curves.

6 Discussion

6.1 The Pressure Revisited

Our present determination of thermodynamic quantities has been based on a calculation of the free energy density through the integration of plaquette expectation values (Eq. 2.8). This approach has been introduced some time ago in order to avoid the use of perturbative relations for the derivatives of coupling constants with respect to the lattice cut-off in spatial (a) and temporal (a_τ) directions [10, 21], which appear when one calculates pressure and energy density from derivatives of the free energy with respect to volume and temperature. The pressure, for instance, is obtained as

$$\frac{p}{T^4} = NN_\tau^4 \left\{ \left[2g^{-2} - \left(\frac{\partial g_\sigma^{-2}}{\partial \xi} - \frac{\partial g_\tau^{-2}}{\partial \xi} \right) \right] (P_\sigma - P_\tau) - 3 \left(\frac{\partial g_\sigma^{-2}}{\partial \xi} + \frac{\partial g_\tau^{-2}}{\partial \xi} \right) \left[2P_0 - (P_\sigma + P_\tau) \right] \right\}, \quad (6.1)$$

where g_σ and g_τ denote the gauge couplings in front of the space-space and space-time plaquettes in the action, $\xi = a/a_\tau$ and the derivatives are taken at $\xi = 1$.^a A comparison of this relation with our new results for the pressure yields one equation for the derivatives of the coupling constants. A second equation is obtained from the well-known connection of the β -function to the sum of derivatives

$$a \frac{dg^{-2}}{da} = -2 \left(\frac{\partial g_\sigma^{-2}}{\partial \xi} + \frac{\partial g_\tau^{-2}}{\partial \xi} \right)_{\xi=1} , \quad (6.2)$$

so that both derivatives may be calculated non-perturbatively. The numerical determination of the derivatives below the transition point, where both the pressure and the plaquette difference $P_\sigma - P_\tau$ are becoming small, will, however, lead to increasing errors. In addition, we expect finite size effects because the transition is of first order in the thermodynamic limit, but continuous on finite lattices. Indeed, we find comparable results above the transition points for $N_\tau = 4, 6$ and 8 , but deviations in the close vicinity of each critical β -value. In Table 3 we list the results from an interpolation of our directly calculated derivative values. As for $SU(2)$ we observe strong deviations from the asymptotic values [21] up to large coupling constant values.

At this point the following remark may be appropriate. The derivatives of the coupling constants are also of importance at the transition point, where they influence the relative size of the gaps in the space-space and space-time plaquettes. Since the pressure is continuous also at the first order transition point, we find from Eq. 6.1 for the differences $\Delta P_{\sigma,\tau}$ between the plaquettes just above and below the transition the following relation

$$\left[g^{-2} - a \frac{dg^{-2}}{da} - \frac{\partial g_\sigma^{-2}}{\partial \xi} \right] \Delta P_\sigma = \left[g^{-2} + a \frac{dg^{-2}}{da} + \frac{\partial g_\tau^{-2}}{\partial \xi} \right] \Delta P_\tau . \quad (6.3)$$

As a consequence, the gaps in P_σ and P_τ will be of the same size for large N_τ , i.e. in the weak coupling region

$$\frac{\Delta P_\sigma}{\Delta P_\tau} = 1 \quad \text{for } N_\tau \rightarrow \infty , \quad (6.4)$$

because the g^{-2} -terms will dominate over the constant derivatives.

^aWe follow here closely the discussion of the $SU(2)$ case presented in [6].

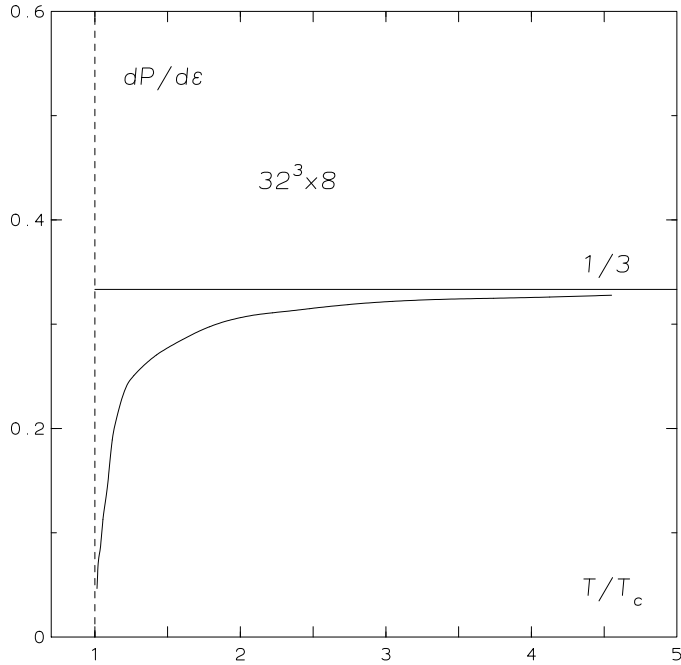


Figure 8: The square of the velocity of sound versus T/T_c for $SU(3)$.

6.2 The Velocity of Sound

A quantity of much interest for the hydrodynamic description of the evolution of a quark gluon plasma, which eventually will get created in ultra-relativistic heavy ion collisions, is the velocity of sound, c_s . It is obtained as

$$c_s^2 = \frac{dp}{d\epsilon} . \quad (6.5)$$

We can determine this quantity easily from the continuum extrapolations of the energy density and the pressure. The result is shown in Fig. 8. We note the rapid decrease of c_s in the vicinity of the deconfinement phase transition, which reflects the rapid rise of the energy density at T_c and the small latent heat at the transition temperature. The transition is *almost second order* in this respect.

6.3 The Gluon Condensate

After a rapid rise close to T_c all normalized thermodynamic observables (i.e. divided by T^4) show a rather slow increase at temperatures above $(2 - 3)T_c$. This suggests that they may be described in terms of functions of a coupling constant $g^2(T)$, which only depends logarithmically on the temperature due to the QCD renormalization group equation. However, it also is clear that the known perturbative expansion of the QCD free energy density [3, 4] is not adequate to describe the numerical results quantitatively. A quantity which is very sensitive to deviations from the perturbative high temperature limit is the trace anomaly of the energy-momentum tensor, $T_\mu^\mu \equiv \epsilon - 3p$. It is connected to the temperature dependent gluon condensate [22] via

$$\epsilon - 3p = \langle G^2 \rangle_{T=0} - \langle G^2 \rangle_T . \quad (6.6)$$

At high temperature the left hand side of this equation has been calculated in continuum perturbation theory [23]

$$\frac{\epsilon - 3p}{T^4} = \tilde{\beta}(g) \left[\frac{(N^2 - 1)}{288} g^4(T) - \frac{N^2 - 1}{16N\pi} \left(\frac{N}{3} \right)^{3/2} g^5(T) + O(g^6) \right] , \quad (6.7)$$

where $\tilde{\beta}$ is defined in Eq. 2.11 and its two first perturbative terms are given by,

$$\tilde{\beta}(g) = 4N[b_0 + b_1 g^2] . \quad (6.8)$$

This shows that $\langle G^2 \rangle_T$ has to be negative and proportional to $g^4(T)T^4$ at high temperature. The first term on the right hand side, $\langle G^2 \rangle_{T=0}$, thus will soon be negligible compared to the second term.

We may re-interpret the numerical results for $\epsilon - 3p$ in terms of the temperature dependence of the gluon condensate. To do so we have to subtract from the numerical results the zero temperature gluon condensate. We use $\langle G^2 \rangle_{T=0} \simeq (1 - 2) \text{ GeV}/\text{fm}^3$ [22], where we allow for quite a large uncertainty. This can be expressed in units of T_c ,

$$\langle G^2 \rangle_{T=0} \simeq (2.5 \pm 1.0) T_c^4 . \quad (6.9)$$

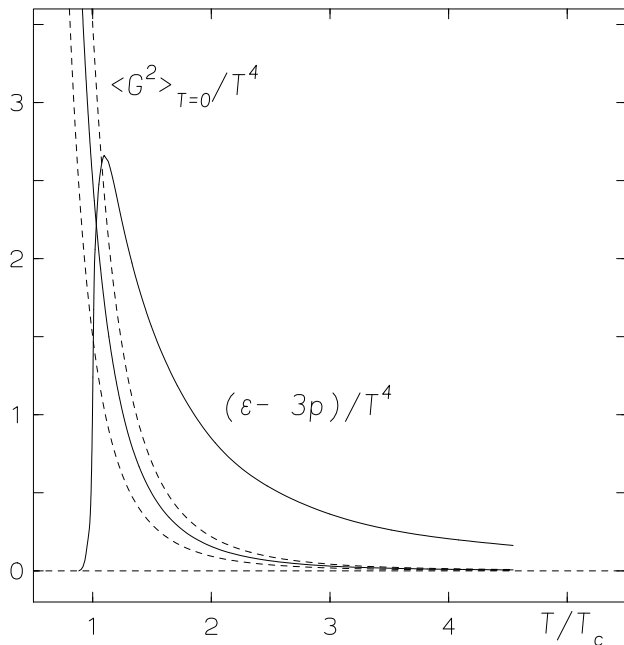


Figure 9: The zero temperature gluon condensate divided by T^4 and $(\epsilon - 3p)/T^4$ versus T/T_c . The dashed lines show the uncertainty of the zero temperature gluon condensate value.

The result for $\langle G^2 \rangle_{T=0}/T^4$ is shown in Fig. 9 together with $(\epsilon - 3p)/T^4$. As can be seen, the exact value of the zero temperature condensate is not important for the high temperature behaviour. Close to T_c the difference $\epsilon - 3p$ is essentially given by $\langle G^2 \rangle_{T=0}$, i.e. the finite temperature condensate $\langle G^2 \rangle_T$, which shows little temperature dependence below T_c , decreases rapidly above T_c and yields the dominant (negative) contribution for $T \gtrsim 2 T_c$. Fig. 9 shows that the contribution of the zero temperature condensate rapidly becomes negligible above T_c . Although this comparison shows that the rise of $(\epsilon - 3p)/T^4$ close to T_c is related to the non-perturbative vacuum contributions to the equation of state, it also makes clear that this is not sufficient to explain the large values for this quantity at temperatures $T \geq 2T_c$. This also cannot easily be explained by the perturbative relation given in Eq. 6.7. If one insists, however, on a comparison with the leading perturbative term only, one has to conclude that the temperature dependent running coupling has to be large, $g^2(T) \simeq 2$ even at $T \simeq 5T_c$. This is consistent with our analysis of the electric and magnetic condensates as well as the spatial string tension, which are discussed in the next two subsections.

6.4 Magnetic and Electric Condensates

The difference $(\epsilon - 3p)/T^4$, as well as ϵ/T^4 and p/T^4 separately, are given by specific combinations of spacelike and timelike plaquette expectation values. The spacelike plaquettes P_σ are related to the spatial components of F_{ij}^2 , $i, j = 1, 2, 3$, i.e. the square of the magnetic field strength. Similarly, the timelike plaquettes are related to the square of the (Euclidean) electric field strength, $F_{0,i}^2$. The different components have been used as an indicator for the behaviour of the magnetic and electric parts of the gluon condensate at high temperature [24]. It therefore is of interest to determine the contributions of space and timelike plaquette expectation values to the difference $\epsilon - 3p$ separately,

$$\begin{aligned}\Delta_\sigma &\equiv 3N_\tau^4 \tilde{\beta} [P_0 - P_\sigma] \quad , \\ \Delta_\tau &\equiv 3N_\tau^4 \tilde{\beta} [P_0 - P_\tau] \quad .\end{aligned}\tag{6.10}$$

As can be seen from the perturbative result for the plaquettes [25], the leading order contributions to $\Delta_{\sigma(\tau)}$ are $O(g^2)$, of opposite sign and equal size

$$\Delta_\tau = -\Delta_\sigma = N_\tau^4 b_0 \frac{N^2 - 1}{2} g^2 (1 - 4I_4) + O(g^4) \quad ,\tag{6.11}$$

with

$$I_4 = \frac{1}{N_\sigma^3 N_\tau} \sum_{n_\mu} \frac{\sin^2(\pi n_4 / N_\tau)}{\sum_{i=1}^3 \sin^2(\pi n_i / N_\sigma) + \sin^2(\pi n_4 / N_\tau)} \quad ,\tag{6.12}$$

where $n_i = 0, 1, \dots, N_\sigma - 1$ and $n_4 = 0, 1, \dots, N_\tau - 1$. While Δ_τ and Δ_σ are $O(g^2)$, these leading order contributions, including all $O(a^n g^2)$ cut-off effects, cancel in $(\epsilon - 3p)/T^4 = \Delta_\sigma + \Delta_\tau$, which is $O(g^4)$. The perturbative expansion of Δ_τ is closely related to that of the energy density. In the continuum limit we find

$$\Delta_\tau = \frac{11N}{720} (N^2 - 1) g^2 + O(g^4) \quad .\tag{6.13}$$

We show Δ_σ and Δ_τ in Fig. 10. We note that up to $T_{\text{peak}} \simeq 1.1T_c$ both terms contribute roughly the same amount to $\epsilon - 3p$. Furthermore, the magnitudes of both quantities remain large even at $5T_c$. In fact, a comparison with Eq. 6.13 shows that $g^2(5T_c) \simeq 1.4$ is needed in order to describe Δ_σ and Δ_τ in terms of the leading order perturbative relation.

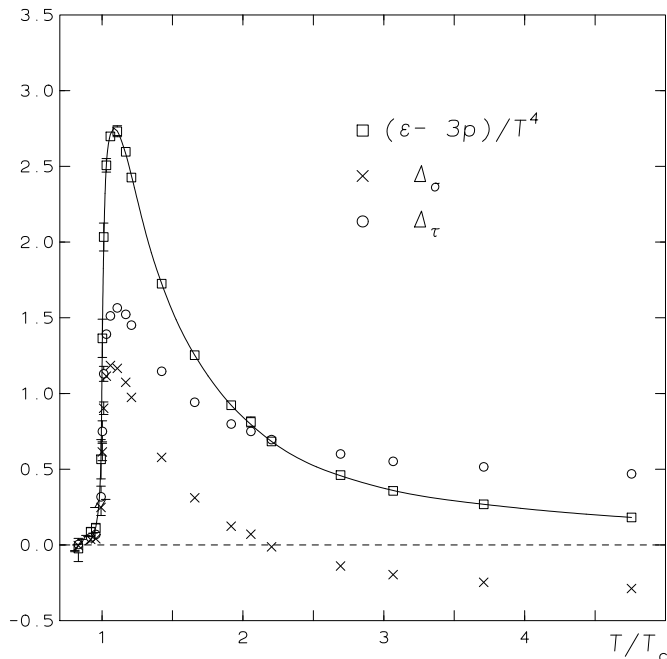


Figure 10: The space- and timelike components Δ_σ and Δ_τ of $(\epsilon - 3p)/T^4$ versus T/T_c on a $32^3 \times 6$ lattice.

6.5 Spatial String Tension

The spatial string tension provides some insight into the structure of the effective three dimensional gauge-Higgs theory, which can be constructed by systematically integrating out heavy modes.

It has been analyzed recently in quite some detail for the $SU(2)$ gauge theory [26]. First results for $SU(3)$ have been reported in [27]. The spatial string tension, σ_s , is extracted from the asymptotic behaviour of large spatial Wilson loops, which

show an area law behaviour even above T_c

$$\langle W(R, S) \rangle \sim e^{-\sigma_s RS} \quad . \quad (6.14)$$

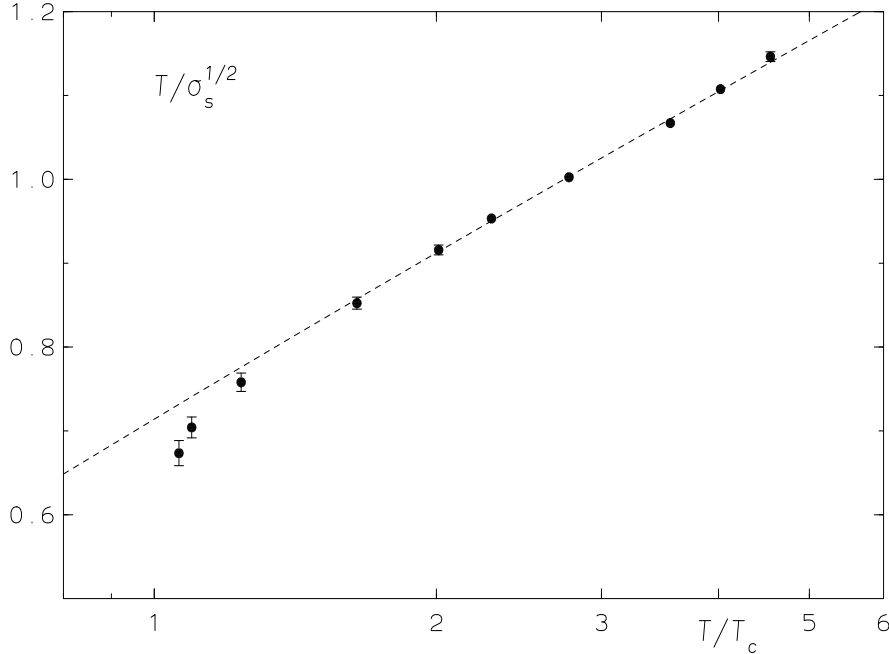


Figure 11: The temperature over the square root of the spatial string tension versus T/T_c for $SU(3)$. The dashed line shows the two-loop-fit according to Eq. 6.15.

We have calculated σ_s at several values of the temperature on our lattices with temporal extent $N_\tau = 8$. At each coupling we have calculated smeared Wilson loops using the method of Ref. [17] up to size $(R, S) = (12, 16)$, taking on-axis as well as off-axis separations for R . We have analyzed these on 1500 configurations and extracted the static potentials $V(R)$ from the logarithm of ratios of Wilson loops^b at each value of the temperature. The spatial string tension has been obtained from a fit of these potentials with an ansatz including a linearly rising term and a Coulomb term. The results for $T/\sqrt{\sigma_s(T)}$ are plotted in Fig. 11. They show that the spatial string tension increases somewhat slower than linear and that the correction is compatible with being logarithmic in T/T_c . We therefore compare the temperature dependence with the expected behaviour

$$\sqrt{\sigma_s(T)} = cg^2(T)T \quad (6.15)$$

^bDetails on the procedure to extract the heavy quark potential can be found in Refs. [17, 27].

and determine the parameter c and $g^2(T)$ from a 2-parameter fit, where we use for $g^2(T)$ the form given by the two-loop renormalization group equation

$$g^{-2}(T) = 2b_0 \ln \frac{T}{\Lambda_\sigma} + \frac{b_1}{b_0} \ln \left(2 \ln \frac{T}{\Lambda_\sigma} \right) , \quad (6.16)$$

with a free Λ_σ -parameter. This fit yields

$$\begin{aligned} c &= 0.566 \pm 0.013 , \\ \frac{\Lambda_\sigma}{T_c} &= 0.104 \pm 0.009 , \end{aligned} \quad (6.17)$$

which is compatible with our earlier determination [27]. We note that these parameters correspond to a coupling $g^2(5T_c) = 1.5$ which is consistent with the value estimated from the behaviour of the electric and magnetic condensates at high temperature.

7 Conclusions

We have systematically analyzed the cut-off dependence of thermodynamic observables of the $SU(3)$ gauge theory at finite temperature. The high statistics evaluation of the energy density and pressure on lattices with temporal extent $N_\tau = 4, 6$ and 8 could be used to extrapolate these quantities to the continuum limit. We find that energy density, entropy density and pressure do approach the high temperature ideal gas limit from below. At temperatures of about $5T_c$ deviations from the ideal gas limit are still about 15%. In fact, the approach to this limit is rather slow, which is in agreement with the expectation that the functional dependence of thermodynamic observables in this regime is controlled by a running coupling which varies with temperature only logarithmically. The analysis of the bulk thermodynamics as well as other observables like the spatial string tension in terms of leading order perturbative relations suggests that this running coupling is larger than unity even at $T \sim 5T_c$.

Within the Wilson formulation of $SU(N)$ gauge theories thermodynamic observables show a cut-off dependence which is $O((aT)^2)$ in the high temperature limit.

This has been used in our extrapolations to the continuum limit. The cut-off dependence can be reduced if one replaces the standard Wilson action by an improved version which, for instance, could be of the form of a Symanzik improved action [20, 28] or a perfect action [29]. This will immediately lead to a reduction of the cut-off dependence of thermodynamic observables in the high temperature ideal gas limit ($T \rightarrow \infty$) [20]. In how far these actions will lead to a reduction of finite cut-off effects also at finite temperatures, in particular for temperatures close to T_c , remains to be seen.

Acknowledgements:

The work has been supported by the DFG under grant Pe 340/3-3. It would not have been possible without the 256-node QUADRICS parallel computer funded by the DFG under contract no. Pe 340/6-1 for the DFG-Forschungsschwerpunkt "Dynamische Fermionen". We thank M. Plagge for the smooth running of this facility.

8 Appendix

In the simulations we have used a Cabibbo-Marinari pseudo-heatbath algorithm with Kennedy-Pendleton updating in the $SU(2)$ subgroups. Every heatbath step was supplemented by 4 to 9 overrelaxed updates, depending on the β value. This then constitutes one sweep. The accumulated statistics on the asymmetric lattices amounts to 20 000 to 40 000 sweeps after thermalization, chosen according to the needed precision in the plaquette data. On the symmetric lattices, between 5000 and 10000 sweeps were sufficient. Plaquettes and Polyakov loops were measured every sweep. For the integrated autocorrelation length, we found a maximum of 250 sweeps for the Polyakov loop right at T_c , dropping quickly to e.g. about 6 sweeps at $1.2T_c$. Autocorrelation times for the plaquette are considerably smaller. The errors on these observables include the integrated autocorrelation lengths. The Wilson loops were measured every 10th sweep. Errors on the local potentials were determined by jackknife with a block length of 100 measurements.

In the tables we give the plaquette expectation values P_0 calculated on symmetric lattices of size 16^4 and 32^4 as well as the spatial (P_σ) and temporal (P_τ) plaquette expectation values on $16^3 \times 4$ and $32^3 \times 6, 8$ lattices. In actual calculations of the pressure and energy density (Eqs. 2.8 and 2.10) we only need the sum ($P_\sigma + P_\tau$). As both quantities are strongly correlated, the error on the sum is the same as on the individual quantities. The same is true for the error on the difference ($P_\sigma - P_\tau$).

| β | $16^3 \times 4$ | | 16^4 |
|---------|-----------------|----------------|---------------|
| | $1 - P_\sigma$ | $1 - P_\tau$ | $1 - P_0$ |
| 5.6500 | 0.537598 (37) | 0.537666 (34) | 0.537642 (36) |
| 5.6600 | 0.540079 (37) | 0.540150 (37) | 0.540073 (38) |
| 5.6700 | 0.542559 (36) | 0.542634 (36) | 0.542401 (43) |
| 5.6800 | 0.545150 (58) | 0.545288 (63) | 0.544748 (35) |
| 5.6825 | 0.545780 (72) | 0.545933 (82) | 0.545345 (42) |
| 5.6850 | 0.546630 (111) | 0.546835 (130) | 0.545862 (44) |
| 5.6900 | 0.548928 (153) | 0.549374 (180) | 0.547021 (32) |
| 5.6925 | 0.549954 (117) | 0.550509 (139) | 0.547564 (37) |
| 5.6950 | 0.551210 (115) | 0.551906 (138) | 0.548088 (34) |
| 5.7000 | 0.552969 (63) | 0.553848 (76) | 0.549214 (29) |
| 5.7050 | 0.554302 (47) | 0.555278 (52) | 0.550205 (32) |
| 5.7100 | 0.555517 (33) | 0.556565 (37) | 0.551265 (33) |
| 5.7200 | 0.557530 (29) | 0.558687 (31) | 0.553357 (32) |
| 5.7300 | 0.559380 (27) | 0.560603 (28) | 0.555353 (30) |
| 5.7500 | 0.562804 (24) | 0.564129 (25) | 0.559121 (41) |
| 5.7700 | 0.565953 (22) | 0.567330 (22) | 0.562692 (27) |
| 5.8000 | 0.570263 (20) | 0.571708 (20) | 0.567651 (21) |
| 5.8500 | 0.576908 (18) | 0.578413 (18) | 0.575115 (33) |
| 5.9000 | 0.582987 (17) | 0.584558 (17) | 0.581792 (21) |
| 5.9500 | 0.588681 (16) | 0.590262 (16) | 0.587977 (19) |
| 6.0000 | 0.594072 (16) | 0.595669 (16) | 0.593678 (24) |
| 6.1000 | 0.604114 (15) | 0.605728 (14) | 0.604115 (16) |
| 6.2000 | 0.613385 (14) | 0.615010 (14) | 0.613647 (20) |
| 6.3000 | 0.622028 (13) | 0.623652 (13) | 0.622450 (14) |
| 6.3500 | 0.626162 (13) | 0.627779 (13) | 0.626610 (10) |
| 6.4000 | 0.630191 (13) | 0.631780 (13) | 0.630663 (19) |
| 6.5000 | 0.637846 (12) | 0.639439 (12) | 0.638411 (20) |
| 6.6000 | 0.645093 (12) | 0.646685 (12) | 0.645712 (17) |
| 6.7000 | 0.652020 (12) | 0.653579 (11) | 0.652635 (16) |
| 6.8000 | 0.658610 (12) | 0.660146 (11) | 0.659236 (7) |

Table 4: The plaquette values on $16^3 \times 4$ and 16^4 lattices.

| β | $32^3 \times 6$ | | $32^3 \times 8$ | | 32^4 |
|---------|-----------------|-----------------|-----------------|-----------------|-----------------|
| | $1 - P_\sigma$ | $1 - P_\tau$ | $1 - P_\sigma$ | $1 - P_\tau$ | $1 - P_0$ |
| 5.800 | 0.5676489 (55) | 0.5676526 (55) | | | 0.5676510 (205) |
| 5.850 | 0.5751411 (58) | 0.5751470 (58) | | | 0.5751226 (54) |
| 5.870 | 0.5779126 (63) | 0.5779266 (59) | | | 0.5778923 (54) |
| 5.890 | 0.5806664 (255) | 0.5807005 (340) | | | 0.5805461 (44) |
| 5.895 | 0.5814918 (272) | 0.5815575 (332) | | | 0.5811950 (46) |
| 5.900 | 0.5822724 (193) | 0.5823817 (233) | | | 0.5818383 (49) |
| 5.910 | 0.5836330 (99) | 0.5837652 (100) | | | 0.5831025 (46) |
| 5.925 | 0.5855217 (42) | 0.5856752 (43) | | | 0.5849659 (46) |
| 5.950 | 0.5885074 (77) | 0.5886900 (80) | | | 0.5879738 (40) |
| 5.980 | 0.5919147 (34) | 0.5921142 (34) | | | 0.5914373 (39) |
| 6.000 | 0.5941102 (47) | 0.5943184 (47) | 0.5936825 (39) | 0.59 36859 (39) | 0.5936846 (39) |
| 6.040 | | | 0.5980109 (34) | 0.59 80153 (36) | 0.5979958 (40) |
| 6.060 | | | 0.6001360 (56) | 0.60 01521 (73) | 0.6000816 (34) |
| 6.065 | | | 0.6006754 (60) | 0.60 06988 (72) | 0.6005991 (35) |
| 6.070 | | | 0.6012168 (43) | 0.60 12460 (46) | 0.6011049 (36) |
| 6.080 | | | 0.6022476 (36) | 0.60 22829 (42) | 0.6021223 (38) |
| 6.100 | 0.6043655 (34) | 0.6045954 (34) | 0.6042724 (40) | 0.60 43161 (40) | 0.6041315 (38) |
| 6.120 | | | 0.6062390 (38) | 0.60 62881 (38) | 0.6060953 (33) |
| 6.140 | | | 0.6081606 (37) | 0.60 82154 (37) | 0.6080241 (35) |
| 6.200 | 0.6137493 (42) | 0.6139905 (40) | 0.6137373 (35) | 0.61 37980 (35) | 0.6136303 (32) |
| 6.300 | 0.6224639 (40) | 0.6227104 (39) | 0.6224809 (33) | 0.62 25500 (33) | 0.6224187 (30) |
| 6.350 | 0.6266149 (35) | 0.6268581 (35) | | | 0.6265895 (30) |
| 6.400 | 0.6306247 (38) | 0.6308739 (37) | 0.6306677 (32) | 0.63 07377 (32) | 0.6306291 (28) |
| 6.550 | 0.6420149 (42) | 0.6422645 (41) | 0.6420717 (30) | 0.64 21439 (30) | 0.6420618 (26) |
| 6.650 | 0.6491184 (31) | 0.6493655 (31) | 0.6491777 (30) | 0.64 92498 (29) | 0.6491831 (19) |
| 6.800 | 0.6591334 (47) | 0.6593798 (46) | 0.6592005 (28) | 0.65 92707 (27) | 0.6592132 (18) |
| 7.000 | 0.6714649 (31) | 0.6717057 (30) | 0.6715327 (27) | 0.67 16058 (27) | 0.6715564 (16) |
| 7.100 | | | 0.6773142 (27) | 0.67 73845 (26) | 0.6773391 (16) |
| 7.200 | | | 0.6828632 (26) | 0.68 29342 (25) | 0.6828924 (16) |

Table 5: The plaquette values on $32^3 \times 6$ and 8 and 32^4 lattices.

References

- [1] L.D. McLerran and B. Svetitsky, Phys. Lett. B98 (1981) 195;
J. Kuti, J. Polonyi and K. Szlachanyi, Phys. Lett. B98 (1981) 199;
J. Engels, F. Karsch, I. Montvay and H. Satz, Phys. Lett. B101 (1981) 89.
- [2] A.D. Linde, Phys. Lett. B96 (1980) 289.
- [3] P. Arnold and C.-X. Zhai, Phys. Rev. D50 (1994) 7603.
- [4] C.-X. Zhai and B. Kastening, Phys. Rev. D52 (1995) 7232.
- [5] E. Braaten and R. Pisarski, Nucl. Phys. B 337 (1990) 569.
- [6] J. Engels, F. Karsch and K. Redlich, Nucl. Phys. B 435 (1995) 295.
- [7] F. R. Brown et al., Phys. Rev. Lett. 61 (1988) 2058.
- [8] K.G. Wilson, Phys. Rev. D 10 (1974) 2445.
- [9] J.Engels, F.Karsch and H.Satz, Nucl. Phys. B 205 [FS5] (1982) 239.
- [10] J. Engels, J. Fingberg, F. Karsch, D. Miller and M. Weber, Phys. Lett. B 252 (1990) 625.
- [11] G. Boyd, J. Engels, F. Karsch, E. Laermann, C. Legeland, M. Lütgemeier and B. Petersson, Phys. Rev. Lett. 75(1995) 4169.
- [12] K. Akemi et al., Phys. Rev. Lett. 71 (1993) 3063.
- [13] S.A. Gottlieb, J. Kuti, D. Toussaint, A.D. Kennedy, S. Meyer, B.J. Pendleton and R.L. Sugar, Phys. Rev. Lett. 55 (1985) 1958.
- [14] N.H. Christ and A.E. Terrano, Phys. Rev. Lett. 56 (1986) 111.
- [15] M. Fukugita, M. Okawa and A. Ukawa, Nucl. Phys. B337 (1990) 181;
Y. Iwasaki, K. Kanaya, T. Yoshié, T. Hoshino, T. Shirakawa, Y. Oyanagi, S. Ichii and T. Kawai, Phys. Rev. D 46 (1992) 4657.

- [16] M. Falconi, E. Marinari, M.L. Paciello, G. Parisi and B. Taglienti, Phys. Lett. 108B (1982) 331; E. Marinari, Nucl. Phys. B235 (1984) 123;
G. Bhanot, S. Black, P. Carter and R. Salvador, Phys. Lett. 183B (1986) 331;
A.M. Ferrenberg and R.H. Swendsen, Phys. Rev. Lett. 61 (1988) 2635; 63 (1989) 1195.
- [17] G. Bali and K. Schilling, Phys. Rev. D46 (1992) 2636.
- [18] J. Fingberg, U. Heller and F. Karsch, Nucl. Phys. B 392 (1993) 493.
- [19] G. Parisi, Proceedings of the XXth Conference on High Energy Physics, Madison 1980;
F. Karsch and R. Petronzio, Phys. Lett. 139B (1984) 403;
A.X. El-Khadra, G. Hockney, A.S. Kronfeld and P.B. Mackenzie, Phys. Rev. Lett. 69 (1992) 729.
- [20] B. Beinlich, F. Karsch and E. Laermann, *Improved Actions for QCD Thermodynamics on the Lattice*, BI-TP 95/33, to be published in Nucl. Phys. B.
- [21] F. Karsch, Nucl. Phys. B205 [FS 5] (1982) 285.
- [22] H. Leutwyler, in Proceedings of the Conference *QCD - 20 years later*, (Edts. P.M. Zerwas and H.A. Kastrup), World Scientific 1993, p. 693.
- [23] J. I. Kapusta, Nucl. Phys. B148 (1979) 461.
- [24] V.K. Mitrjushkin, A.M. Zadorozhny and G.M. Zinovjev, Phys. Lett. B215 (1988) 371;
S.H. Lee, Phys. Rev. D40 (1989) 2485;
H.G. Dosch, H.J. Pirner and Yu.A. Simonov, Phys. Lett. B349 (1995) 335.
- [25] U. Heller and F. Karsch, Nucl. Phys. B251[FS13] (1985) 254.
- [26] L. Kärkkäinen, P. Lacey, D.E. Miller, B. Petersson and T. Reisz, Phys. Lett. B312 (1993) 173;
G.S. Bali, J. Fingberg, U.M. Heller, F. Karsch and K. Schilling, Phys. Rev. Lett. 71 (1993) 3059.
- [27] F. Karsch, E. Laermann and M. Lütgemeier, Phys. Lett. B346 (1995) 94.

- [28] K. Symanzik, Nucl. Phys. B226 (1983) 187 and Nucl. Phys. B226 (1983) 205.
- [29] P. Hasenfratz and F. Niedermayer, Nucl. Phys. B414 (1994) 785;
T. DeGrand, A. Hasenfratz, P. Hasenfratz and F. Niedermayer, Nucl. Phys. B454 (1995) 587 and 615.